



High link performance of Brillouin-loss based microwave bandpass photonic filters

ANDRI MAHENDRA,^{1,2} YANG LIU,^{1,2} ERIC MAGI,^{1,2} AMOL CHOUDHARY,^{1,2}
DAVID MARPAUNG,^{1,2,3} AND BENJAMIN J. EGGLETON^{1,2*}

¹*Institute of Photonics and Optical Science (IPOS), School of Physics, University of Sydney NSW 2006, Australia*

²*The University of Sydney Nano Institute (Sydney Nano), University of Sydney, NSW 2006, Australia*

³*Present address: The Faculty of Science and Technology, University of Twente, Enschede, Netherlands*

*benjamin.eggleton@sydney.edu.au

Abstract: We present a high link-performance multi-band microwave photonic filter based on stimulated Brillouin scattering (SBS) loss responses. The bandpass filter response is formed by suppressing the out-of-band signal using multiple broadened SBS loss responses, which avoids introducing additional noise in the passband. The low-noise SBS bandpass filter is implemented in an optimized high-performance MWP link, which enabled the demonstration of filter functionalities with a low noise figure, reconfigurability, and high resolution. A noise figure of 18.9 dB is achieved in the passband with a filter bandwidth of 0.3 GHz at a central frequency of 14 GHz, with a link gain of -13.9 dB and a spurious free dynamic range of 106 dB.Hz^{2/3}. Bandwidth reconfiguration from 0.1 GHz to 1 GHz and multi-bandpass responses are also demonstrated.

© 2018 Optical Society of America under the terms of the [OSA Open Access Publishing Agreement](#)

1. Introduction

Microwave photonic (MWP) systems have attracted considerable interest in the past decade for RF applications such as broadband wireless access networks, satellite, and modern radar systems enabling low loss, immunity to electromagnetic interference (EMI), broad bandwidth, reconfigurability and tunability [1,2]. One of the important building blocks in MWP systems is the bandpass MWP filter that can perform the equivalent task of an ordinary electrical microwave filter within a radio frequency (RF) system or link [3,4], exhibiting the advantages of broad processing bandwidth and wide-range tunability offered by photonics.

MWP filters based on stimulated Brillouin scattering (SBS) are attractive for MWP applications, due to the high spectral resolution and optically programmable responses offered by the Brillouin processing [5]. SBS is a nonlinear optical process that results in a narrowband gain at the frequency shifted from the pump by $-\Omega$ while a narrowband loss response at the frequency shifted by $+\Omega$, where Ω is the Brillouin frequency shift [6]. SBS enables a unique photonic processing capability with an ultra-narrow natural bandwidth of ~ 30 MHz which can be further reduced to the level of ~ 3 MHz using additional filter shaping techniques [7,8]. SBS has enabled a wide range of functionalities and applications, together with the potential of integration [9–13]. Although impressive demonstrations of functionalities have been obtained using SBS filters, such filters need to meet the demanding system performance required in real-world applications, particularly link gain and noise Fig [14,15]. Previous realization of MWP bandpass filters based on SBS gain response have exhibited excessive in-band noise induced by the spontaneous emission associated with the SBS amplifications, leading to a high noise figure penalty, which makes the SBS-based MWP filter impractical for real-world applications [16–18]. There have been recent efforts to mitigate the additional SBS noise in the passband of an optical filter, using broadband SBS loss to suppress out-of-band signals, which enables the creation of a bandpass response, while avoiding added SBS amplification noise in the passband [19–21]. This approach offers a

potentially noise-free passband solution for tunable microwave filter technology but needs to be implemented in a high-performance microwave photonic link and to provide desired programmable multi-bandpass MWP filter functionality. Considering the high-resolution RF signal processing that SBS enables, there is a need to merge the high link-performance, high-resolution processing and response programmability for SBS-based RF photonic filters that can meet the requirements of practical microwave applications.

In this paper, we demonstrate high link-performance SBS-based microwave photonic filters. By combining an optimized high performance analog photonic link with low noise SBS-based filters, we achieve a significant step towards practical MWP signal processing, for the first time, enabling the synthesis of high link-performance, tunable and reconfigurable SBS-based microwave photonic filters, with up to 10 passbands. These results suggest new ways of creating high-performance, agile filters for future microwave photonic sub-systems for wireless communication and defense applications.

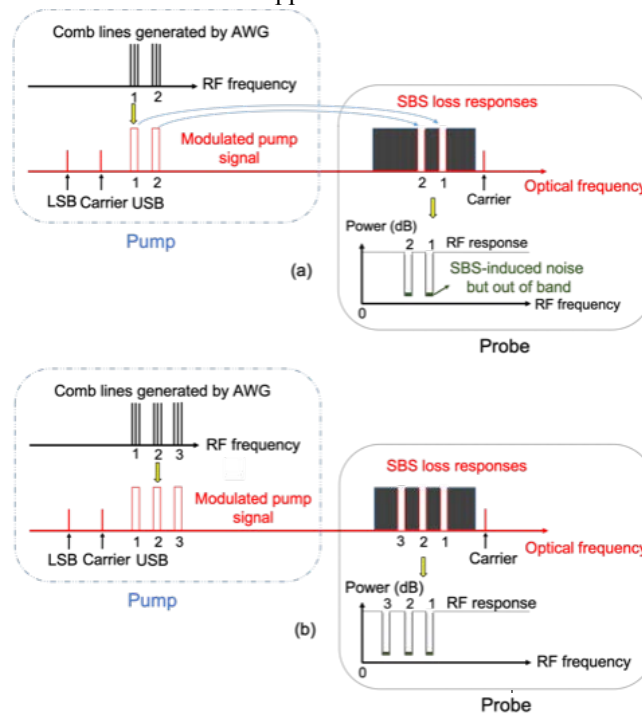


Fig. 1. Schematic of the operation principle of the SBS-losses-based filter. (a) RF response of single bandpass (right) at probe created from pump control (left); AWG comb lines generation (top left), SBS loss responses in optical domain (top right) by single side band modulation on upper side band (USB) with lower side band (LSB) and carrier suppression. (b) Multiple bandpass filter formation at probe created from multiple comb lines from pump by adding comb lines group (3) using AWG (top left) therefore adding SBS loss responses (top right).

2. Principle

Figure 1 shows the principle of the low-noise bandpass filter formed by SBS-based losses, without introducing extra losses in the filter passband. In this approach, the noise figure of the filter passband is unaffected by the noise generated through the SBS amplification process [19]. This contrasts with the MWP bandpass filter creation using SBS gain, which processes the signal of interest and introduces additional noise in the passbands [20].

This technique suppresses the out-of-band signal of the passband by the broadened optical pump controlled by electrical arbitrary waveform generator (AWG) and the suppression depends on the SBS loss responses. The signals of interest are accommodated in the passband and the passband bandwidth can be adjusted by tuning the spacing of the comb lines group (1

and 2) in Fig. 1(a) and 1(b). To obtain broadband tunability, the SBS filter configuration could be combined with a tunable coarse optical filter, such as a fiber Bragg grating (FBG), with significantly reduced filter requirements [19]. To create multiple passbands and form different filter shape, additional pumps (comb lines group 3) with various frequencies and separations can be programmed by an AWG.

To achieve high link-performance SBS-losses-based filter, we first implement a high performance MWP link as the basis of the link performance of the MWP filter. The state-of-the-art fiber-based MWP links without RF pre-amplification and signal processing functionality have been reported to achieve a good link performance, typically exhibiting an RF link gain of 10 dB, noise figure (NF) of <10 dB, and spurious free dynamic range (SFDR) of >120 dB.Hz^{2/3} [22,23]. However, combining the high link-performance architecture with signal processing functionalities in MWP systems requires careful considerations both of the MWP link and of the photonic functional units, to minimize introducing excessive losses and noise that will significantly deteriorate the link performance, which is crucial for the overall MWP system performance [24,25].

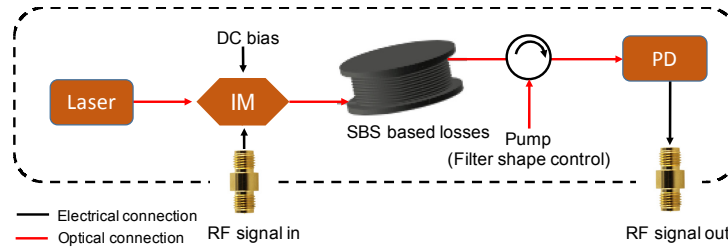


Fig. 2. Schematic of the high-performance microwave photonic link that can accommodate SBS to implement MWP filter. This filter is treated as a black box interfaced with one RF input port and one RF output port. The RF signals are processed by an optical link employing an intensity modulator with SBS process in the optical fiber. In optical link, long fiber spool and pump signal can be considered to implement the filter shape control. IM: intensity modulator; PD: photodetector.

The analog link performance of the filter is important because it will determine the quality and fidelity of the RF signal passing through MWP link. Figure 2 shows the conceptual architecture of the MWP filter based on SBS losses incorporated in the analog photonic link with an optical pump block for filter shape control and photodetector (PD).

A general front-end in an MWP photonic link configuration consists of a laser and an external modulator for the electrical to optical (E-O) conversion. To achieve a low noise figure, avoiding to introduce additional noises to the MWP is equally important as achieving a good link gain, which can be improved by using appreciable laser power and high-efficient modulation and photodetection [26]. The noise figure in decibels is calculated by the expression given by

$$NF = P_N - G + 174 \quad (1)$$

The noise figure is defined by the [Eq. (1)], in which the $10\log_{10}(kT) \approx -174$ dBm/Hz for $T = 290$ K and $G = 10\log_{10}(g)$ is the gain expressed in dB and P_N is the measured total noise power spectrum density as described detail in [22].

In addition, a high modulation linearity determined by the modulator transfer function is also important in an analog photonic link (APL) [27] to minimize the signal distortions, which is measured by the SFDR [1]. The SFDR_n (dB.Hz^{2/3}) performance is calculated by [Eq. (2)] where the NF and IIP_n are the obtained noise figure and the order of input intercept point.

$$SFDR_n = \frac{n-1}{n}(IIP_n - NF + 174) \Rightarrow SFDR_3 = \frac{2}{3}(IIP_3 - NF + 174) \quad (2)$$

An appreciable received optical power is expected to maintain a good link gain, but on the other hand the high average DC current will lead to a high RIN noise (proportional to the square of the DC current), which dominates over the shot noise limit arising from random optical field detection (proportional to the DC photocurrent). The link performance optimization techniques help relax these performance requirements of optical components, typically the low-biasing technique [28–32]. By applying the low-biased modulation configuration, the dominant RIN noise is reduced more quickly than the output signal due to the different dependences of the DC bias voltage of the MZM [26].

To maintain the signal-to-noise ratio (SNR) that will translate into a low noise figure, high-power optical source and necessary signal amplification are needed to offset the losses in the link and the signal conversion efficiency. In addition, one approach to increasing the link gain and reducing the noise figure is by employing a low noise RF amplifier in the frontend of the link [27].

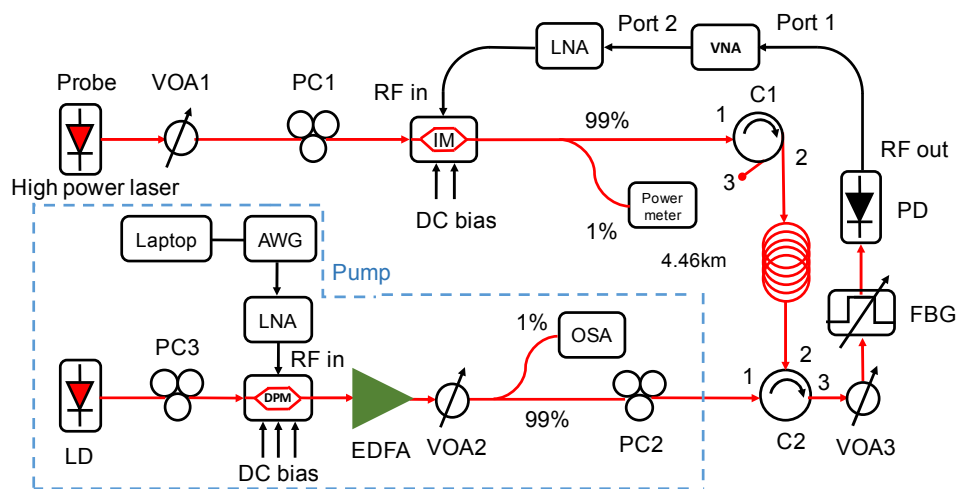


Fig. 3. Schematic of SBS losses based filter experiment setup. Top-half of the setup is the probe. The bottom side of the figure shows the pump of the filter setup including laser diode (LD), polarization controller (PC2, PC3), dual parallel Mach Zehnder modulator (DPMZM) or IQ modulator (IQM), arbitrary waveform generator (AWG), low noise amplifier (LNA), erbium-doped fiber amplifier (EDFA), high resolution optical spectrum analyzer (OSA), circulator (C2), and a fiber Bragg grating filter (FBG).

3. Experiments and results

3.1 MWP link optimization

Figure 3 shows the experimental setup to demonstrate the filter operation. A high-power laser (RIO Grande) with a maximum output power of 32 dBm is used as the probe laser. A variable optical attenuator (VOA1) is connected to the laser output for power control. A polarization controller (PC1) is positioned to align the polarization to the main axis of the MZM (EOSpace 20 GHz). The MZM DC half-wave voltage is measured to be 4.4 V with 5 dB optical insertion loss. The RF input is generated by vector network analyzer (Agilent VNA) with amplification provided by a low noise amplifier (LNA Mini-Circuits ZVA-213 + 800 MHz to 21 GHz with a typical noise figure of 3 dB and output third order intercept point of +33 dBm). 1% of the output light from the intensity modulator is tapped for power monitoring while 99% passes through a circulator (C1). The C1 provided is used to isolate the counter-propagating optical pump at Port 1. Meanwhile, Port 3 of C1 can be used to monitor the transmission of the optical pump. A 4.46-km fiber is used as the SBS medium. The output of this fiber is then connected to circulator (C2) before it is linked to a variable optical attenuator

(VOA3). This optical signal is detected by a photodetector (InGaAs APIC 20 GHz with 0.95 A/W responsivity and 50 Ohm termination), which converts the optical signal to the RF signal. The RF output from the photodetector is collected by the VNA to produce S_{21} response of the MWP link.

We reduced the noise power by low biasing the MZM and increasing the link gain by using RF amplification. The MZM sets at low bias angle of $0.05 (\phi_B/\pi)$. The ϕ_B is the bias angle of the modulator. As a result of inserting the RF LNA before the modulator, the gain improved without significant increase in noise from the RF input source. By measuring the S_{21} response, noise power density, the performance of the analog photonic link can be analyzed and optimized.

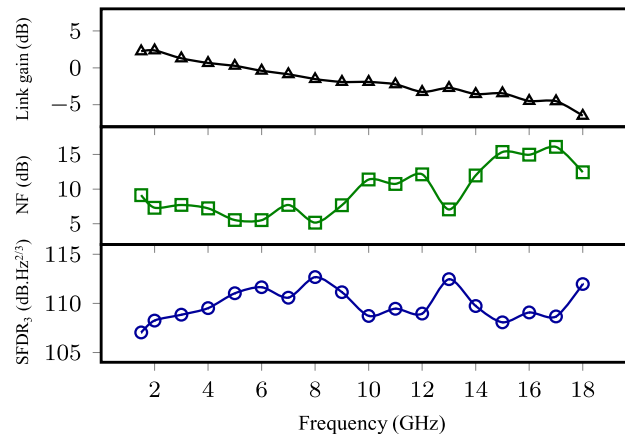


Fig. 4. Link gain, Noise Figure and Spurious-free Dynamic Range vs. Frequency of the microwave photonic link.

The experiments were conducted at frequencies of up to 18 GHz. Figure 4 shows the link performance without the filter functionalities. The analog photonic link showed an average NF between 5 and 10 dB for frequencies < 10 GHz with RF gain > -1.9 dB. We performed a two-tone test with 10 MHz tone spacing and measured the 3rd order intercept points and thus the SFDR. Figure 4 (blue) depicts the SFDR₃ measurement result with different frequencies from 1.5 GHz to 18 GHz. The average SFDR₃ performance from 1.5 GHz to 18 GHz is 109.8 dB.Hz^{2/3}. This performance is obtained by combining high power laser input, a low-biased configuration of a Mach Zehnder modulator (MZM) and by using a low noise amplifier (LNA) at the input of modulator.

3.2 Reconfigurable SBS losses-based filter

Here, we incorporate the SBS-based functionality with the optimized high-performance link described in the previous section, as the scheme showed in Fig. 3. An SBS pump at 1550 nm was generated and injected into a dual parallel Mach Zehnder modulator (EOSpace DPMZM). For the SBS pump, we used a semiconductor laser diode (Teraxion Pure Spectrum at $\lambda = 1550$ nm) with 100 mW of optical power, connected via a polarization controller. The AWG was used to generate electrical comb lines which modulate the pump laser through single-sideband suppressed carrier modulation via the DPMZM to form desired SBS pump lines, allowing arbitrary control of the filter shape.

The three bias voltages of the DPMZM were adjusted using a programmable multichannel voltage supply with 16-bit accuracy (Nicslab XPOW-3AX max 30 V). The modulated optical signal from the DPMZM was amplified by an erbium-doped fiber amplifier (EDFA, Amonics) with a maximum output power of 500 mW. The amplified signal then passed through a variable optical attenuator (VOA2) before it goes to a 99/1% coupler and

polarization controller (PC2). A high-resolution optical spectrum analyzer (Finisar 1500S) was used to monitor the lower sideband suppression signal and for spectrum analysis. The output signal from PC2 was injected to the link via an optical circulator (C2). The link signal output and the SBS filter from the circulator (port 3) was detected using a high-speed photodetector (APIC 20 GHz - 50 Ohm termination) with 0.95 A/W responsivity. The input power to the detector was controlled using a variable optical attenuator (VOA3). The FBG locating before the PD is used to remove one of the upper sideband of the modulated optical signals. Therefore, the SBS-loss-induced optical response can be mapped to the RF domain. Consequently, the insertion of FBG also introduces a link gain penalty of 10.8 dB RF (5.4 dB optical loss) and a corresponding increase in noise figure. The FBG used in our experiments was an in-house developed filter with 16 GHz bandwidth, 20 dB rejection. For the measurements of the filter responses, a frequency-swept RF signal was supplied from and measured on a 43.5 GHz by vector network analyzer (Agilent PNA 5224A).

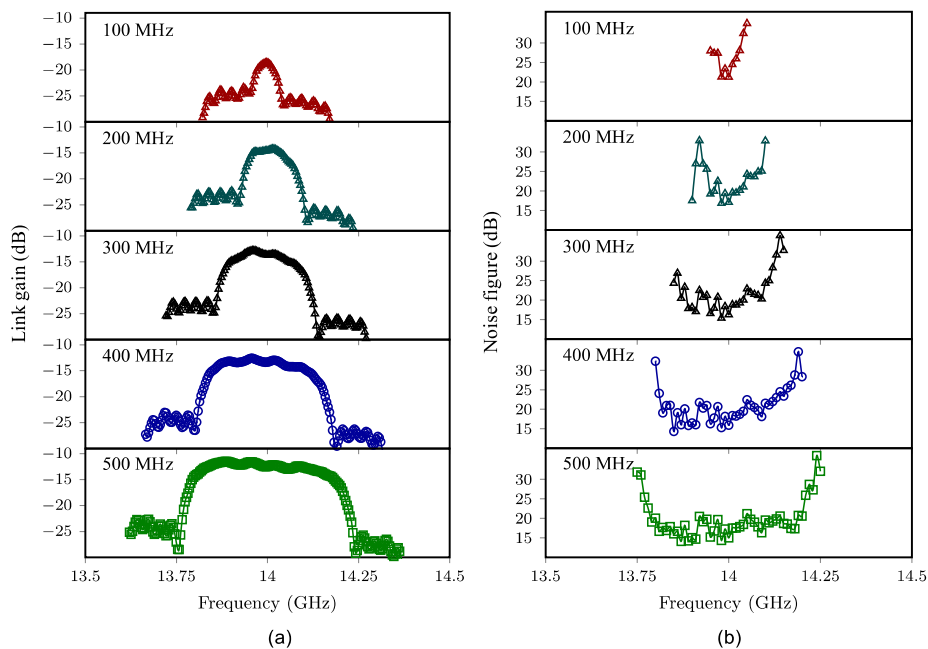


Fig. 5. Filter broadening experiment results from 0.1 GHz to 0.5 GHz at a central frequency of 14 GHz (a) Link gain (dB) vs. frequency (b) Noise figure (dB) vs. frequency.

Reconfiguration of the filter bandwidth was achieved by adjusting the comb line generation via the AWG program. Figure 5(a) shows filter broadening experiment result at a central frequency of 14 GHz with passband bandwidth from 0.1 GHz to 0.5 GHz. The highest link gain of -11 dB was obtained at 500 MHz. At a narrower passband bandwidth at 100 MHz, the link gain was measured to be -18.5 dB due to overlapping between SBS loss responses on both sides of the passband. Figure 5(b) presents the corresponding noise figure performance of filter formation from Fig. 5(a). The lowest noise figure was obtained at around 15 dB with 500 MHz passband bandwidth. The noise figure for 100 MHz passband bandwidth was 20 dB. These figures show that the narrower the bandwidth, the link gain of the filter also decreases therefore the corresponding noise figure increases, which is consistent with the [Eq. (1)].

Figure 6(a) and Fig. 6(b) show the reconfigurable filter with different bandwidths (0.1 GHz to 0.5 GHz) and noise figure measurement results at different central frequencies. The filters were independently created for each bandwidth by the AWG. The 2.3 dB flatness was

measured within 400 MHz response of 0.5 GHz passband bandwidth as shown in Fig. 6 (a). The flatness is the natural response or link gain of S_{21} measurement. The ripple on this flat response could be affected by the noise and power reduction from the RF cable transmission and frequency dependent on components such as the LNA and the photodetector. The lowest noise figure of 15.7 dB at the passband was achieved with 0.5 GHz passband bandwidth at frequency of 14 GHz as shown in Fig. 6(b) with -13.4 dB link gain.

The SFDR₃ at 0.3 GHz passband bandwidth was measured using a two-tone test to be 106 dB.Hz^{2/3} at 14 GHz with 18.9 dB noise figure and -13.9 dB link gain. The SFDR₃ was 105 dB.Hz^{2/3} for 0.1 GHz passband with 20.6 dB noise figure and -17.3 dB link gain at 14 GHz. The noise figure degradation compared to the link without any functionalities is due to the FBG that induces optical insertion losses (2.4 dB) and suppresses the optical upper side (3 dB loss) thereby causing additional 10.8 dB penalty in the RF link gain.

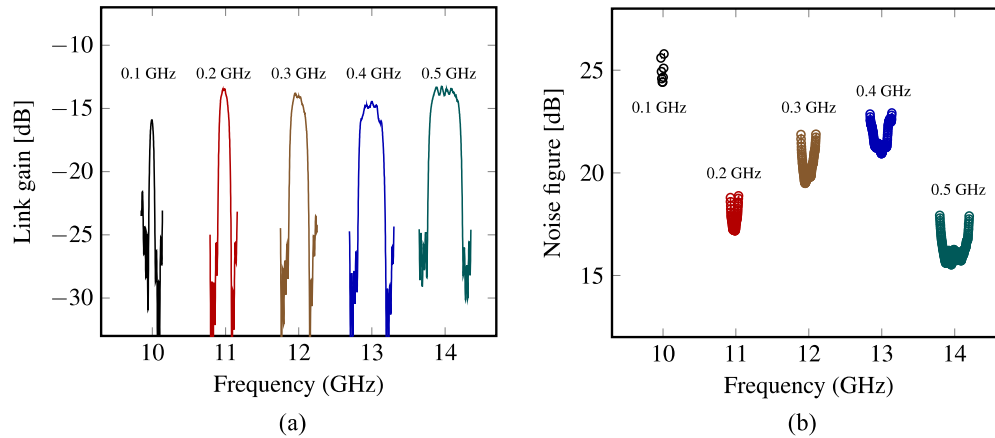


Fig. 6. Filter broadening experiment results from 0.1 GHz to 0.5 GHz and noise figure in the passband at central frequencies between 9 GHz and 15 GHz. (a) Link gain (dB) vs. frequency. (b) Noise figure (dB) vs. frequency.

3.3 Multiband SBS losses based-filter

Multi-band filter is important for RF applications where RF signals of interest are accommodated in different frequency channels and crosstalk need to be isolated. To demonstrate the flexible programmability and tunability of SBS-based filter for multi-band generation, multi-passband filters were generated simultaneously through AWG. Figure 7(a) and 7(b) depict the filter with bandwidth from 0.1 GHz to 1 GHz and noise figure measurement results.

To emulate real-life signals, a strong interfering signal was passed through our filter with a weak signal. Figure 8 shows the demonstration of interference signal rejection with 200 MHz passband filter at a central frequency of 14 GHz. The interferer signal (14.2 GHz) was reduced by 32 dB.

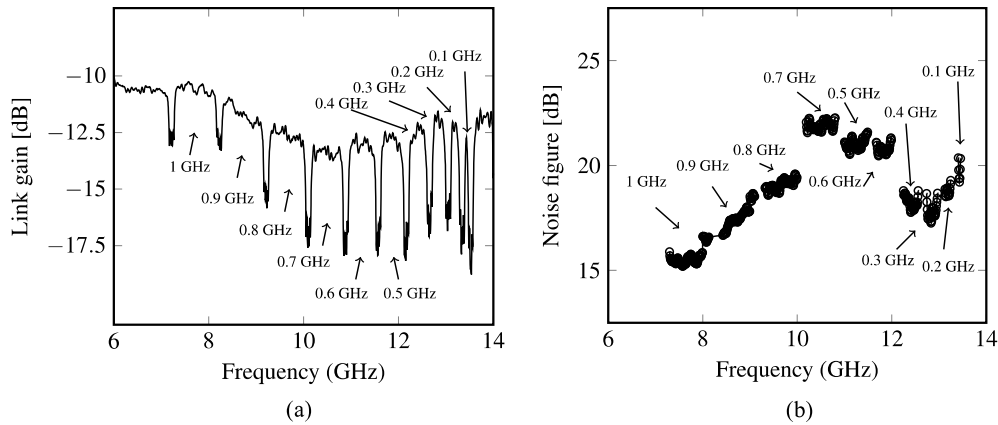


Fig. 7. Filter broadening experiment results from 100 MHz to 1 GHz and noise figure. (a) Link gain (dB) vs. Frequency. (b) Noise figure (dB) vs. Frequency.

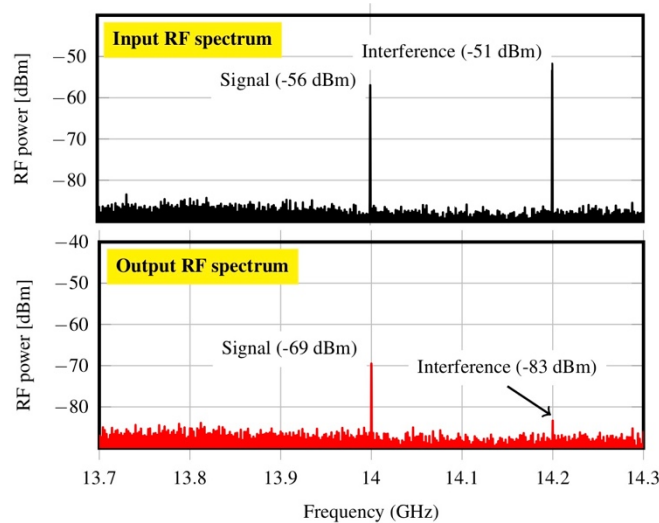


Fig. 8. Bandpass filter demonstration with interference signal

4. Discussion

The present filter demonstration shows the natural flat-top passband from the link response. The ripples at the bandstop is due to the strength/amplitude variation of the comb-like pump lines generated in the electrical and optical components and fiber [21]. Although the stopbands are out of the frequency range of the signal of interest, the responses can be further improved using feedback control as described in [16,33].

One can note that the rejection of the filter stopband is determined by the strength of the SBS loss and polarization, which is limited by the optical pump power, especially in a filter configuration implemented by multiple broadband stopbands.

To relax the stringent requirement in high pump power, an additional optical filter with lower spectral resolution can be used to provide band spectrum rejection as pre-processing operations, followed by the SBS-loss-based high-resolution spectrum processing [19]. This configuration can pair the coarse processing capability of the pre-processing optical filter offers with the high resolution provided by SBS, allowing for broadband operation and high-resolution signal processing with a lower pump power consumption. To further scale the frequency filter range and to increase rejection, high bandwidth digital to analog conversion

and advanced feedback control on AWG can be applied on comb-line generation [33]. The minimum noise figure obtained in our filter was 15 dB at 0.5 GHz passband with -11 dB link gain at 14 GHz. However, we note that with passband lower than 0.3 GHz, the link gain reduces to around -17.1 dB with 0.1 GHz passband at 14 GHz. This is due to the overlapping between SBS loss responses on either side of the passband for narrow bandwidths. Therefore, it affects the link gain and noise figure. Moreover, since the noise figure calculated by the obtained filter link gain and measured total noise power spectrum density (P_N) on an electrical spectrum analyzer, it provides less accurate measurement. Further measurement using the Y-factor or direct-noise method needs to be performed to get more accurate measurement [34].

We note that a high RF power of the input signal to the modulator with low noise amplification would improve the link gain and therefore the noise figure, but on the other hand might also lead to an increase in the nonlinearity from the LNA, which reduces the dynamic range. Therefore, a trade-off exists between the noise figure and the dynamic range, which needs to be considered when choosing the signal gain amplification.

5. Conclusions

In conclusion, we have reported an agile MWP multi-bandpass filter using SBS based losses with minimum-low noise figure of 18.9 dB with SFDR₃ of 106 dB.Hz^{2/3} and -13.9 dB insertion loss. The filter exhibits a unique performance through the combination of the high link performance and filter functionality including tuning range, resolution, and reconfigurability. Combining the key performance of the analog photonic link and low noise SBS filter is a significant step for high-resolution MWP signal processing.

The miniaturization of the SBS medium provides a promising approach to significantly reducing the footprint of the proposed low-loss filter, which is of great interest to space and mobile applications where compactness and light weight is required. By employing the record-high-performance SBS photonic chip in the MWP link, the form factor or the key component of the filter can be reduced to the centimeter scale [8,9,35]. By integrating key components such as silicon-based lasers, modulators and detectors with on-chip functional SBS circuits, a monolithic photonic chip will be an attractive platform to achieve high link performance and flexible filters with unprecedented compactness.

Funding

Lockheed Martin (University of Sydney contract); ARC's DECRA (DE17010058) Fellowship; ARC Centre of Excellence (CUDOS, CE110001018); ARC Laureate Fellowship (FL120100029); U.S. Office of Naval Research Global (N62909-18-1-2013).

Acknowledgment

This work is supported by Lockheed Martin under a University of Sydney contract. A. Choudhary acknowledges the ARC's DECRA (DE17010058) Fellowship. B. J. Eggleton acknowledges ARC support in the context of the Centre of Excellence (CUDOS, CE110001018); Laureate Fellowship (FL120100029). The authors would also like to thank U.S. Office of Naval Research Global for financial support (grant no. N62909-18-1-2013).

References

1. V. J. Urick, J. D. McKinney, and K. J. Williams, *Fundamentals of Microwave Photonics* (Wiley, 2015).
2. J. Yao, "Microwave photonics," *J. Lightwave Technol.* **27**(3), 314–335 (2009).
3. J. Capmany, B. Ortega, and D. Pastor, "A tutorial on microwave photonic filters," *J. Lightwave Technol.* **24**(1), 201–229 (2006).
4. J. Ge and M. P. Fok, "Passband switchable microwave photonic multiband filter," *Sci. Rep.* **5**(1), 15882 (2015), doi:10.1038/srep15882.
5. M. Merklein, A. Casas-Bedoya, D. Marpaung, T. F. S. Buttner, M. Pagani, B. Morrison, I. V. Kabakova, and B. J. Eggleton, "Stimulated Brillouin Scattering in Photonic Integrated Circuits: Novel Applications and Devices," *IEEE J. Sel. Top. Quantum Electron.* **22**(2), 336–346 (2016).

6. D. Marpaung, M. Pagani, B. Morrison, and B. J. Eggleton, "Nonlinear Integrated Microwave Photonics," *J. Lightwave Technol.* **32**(20), 3421–3427 (2014).
7. S. Preussler, A. Wiatrek, K. Jamshidi, and T. Schneider, "Brillouin scattering gain bandwidth reduction down to 3.4MHz," *Opt. Express* **19**(9), 8565–8570 (2011).
8. A. Wiatrek, S. Preussler, K. Jamshidi, and T. Schneider, "Frequency domain aperture for the gain bandwidth reduction of stimulated Brillouin scattering," *Opt. Lett.* **37**(5), 930–932 (2012).
9. A. Byrnes, R. Pant, E. Li, D.-Y. Choi, C. G. Poulton, S. Fan, S. Madden, B. Luther-Davies, and B. J. Eggleton, "Photonic chip based tunable and reconfigurable narrowband microwave photonic filter using stimulated Brillouin scattering," *Opt. Express* **20**(17), 18836–18845 (2012).
10. D. Marpaung, B. Morrison, M. Pagani, R. Pant, D.-Y. Choi, B. Luther-Davies, S. J. Madden, and B. J. Eggleton, "Low-power, chip-based stimulated Brillouin scattering microwave photonic filter with ultrahigh selectivity," *Optica* **2**(2), 76 (2015).
11. R. Van Laer, B. Kuyken, D. Van Thourhout, and R. Baets, "Interaction between light and highly confined hypersound in a silicon photonic nanowire," *Nat. Photonics* **9**(3), 199–203 (2015).
12. E. A. Kittlaus, N. T. Otterstrom, and P. T. Rakich, "On-chip inter-modal Brillouin scattering," *Nat. Commun.* **8**, 15819 (2017).
13. B. Morrison, A. Casas-Bedoya, G. Ren, K. Vu, Y. Liu, A. Zarifi, T. G. Nguyen, D.-Y. Choi, D. Marpaung, S. J. Madden, A. Mitchell, and B. J. Eggleton, "Compact Brillouin devices through hybrid integration on silicon," *Optica* **4**(8), 847–854 (2017).
14. E. A. Kittlaus, P. Kharel, N. T. Otterstrom, Z. Wang, and P. T. Rakich, "RF-photonic Filters via On-chip photonic-phononic emit-receive operations." *J. Lightwave Technol.*, vol. 1, 2018.
15. A. Choudhary, I. Aryanfar, S. Shahnia, B. Morrison, K. Vu, S. Madden, B. Luther-Davies, D. Marpaung, and B. J. Eggleton, "Tailoring of the Brillouin gain for on-chip widely tunable and reconfigurable broadband microwave photonic filters," *Opt. Lett.* **41**(3), 436–439 (2016).
16. Y. Stern, K. Zhong, T. Schneider, R. Zhang, Y. Ben-Ezra, M. Tur, and A. Zadok, "Tunable sharp and highly selective microwave-photonic band-pass filters based on stimulated Brillouin scattering," *Photon. Res.* **2**(4), B18 (2014).
17. W. Wei, L. Yi, Y. Jaouën, and W. Hu, "Bandwidth-tunable narrowband rectangular optical filter based on stimulated Brillouin scattering in optical fiber," *Opt. Express* **22**(19), 23249–23260 (2014).
18. A. Choudhary, Y. Liu, D. Marpaung, B. J. Eggleton, "Brillouin filtering with enhanced noise performance and linearity using anti-stokes interactions," *CLEO: Science and innovation conference*, 2018.
19. C. Feng, S. Preussler, and T. Schneider, "Sharp tunable and additional noise-free optical filter based on Brillouin losses," *Photon. Res.* **6**(2), 132 (2018).
20. M. F. Ferreira, J. F. Rocha, and J. L. Pinto, "Analysis of the gain and noise characteristics of fiber Brillouin amplifiers," *Opt. Quantum Electron.* **26**(1), 35–44 (1994).
21. M. Choi, I. C. Mayorga, S. Preussler, and T. Schneider, "Investigation of gain dependent relative intensity noise in fiber Brillouin amplification," *J. Lightwave Technol.* **34**(16), 3930–3936 (2016).
22. D. Marpaung, C. Roeloffzen, R. Heideman, A. Leinse, S. Sales, and J. Capmany, "Integrated microwave photonics," *Laser Photonics Rev.* **7**(4), 506–538 (2013).
23. H. V. Roussel, M. D. Regan, J. L. Prince, C. H. Cox, J. X. Chen, W. K. Burns, G. E. Betts, and E. I. Ackerman, "Gain, noise figure and bandwidth-limited dynamic range of a low-biased external modulated link," *Microwave Photonics (MWP), IEEE International Topical Meeting on*, vol. 1, pp. 84–87, Oct, 2007.
24. Y. Liu, J. Hotten, A. Choudhary, B. J. Eggleton, and D. Marpaung, "All-optimized integrated RF photonic notch filter," *Opt. Lett.* **42**(22), 4631–4634 (2017).
25. Y. Liu, D. Marpaung, A. Choudhary, and B. J. Eggleton, "Lossless and high-resolution RF photonic notch filter," *Opt. Lett.* **41**(22), 5306–5309 (2016).
26. S. Iezekiel, *Microwave Photonic Devices and Applications* (Wiley, 2009).
27. V. J. Urick, J. F. Diehl, J. M. Singley, C. E. Sunderman, and K. J. Williams, "Long-reach analog photonics for military applications," *Opt. Photonics News* **25**(10), 36–43 (2014).
28. M. L. Farwell, W. S. C. Chang, and D. R. Huber, "Increased linear dynamic range by low biasing the Mach Zehnder modulator," *IEEE Photonics Technol. Lett.* **5**(7), 779–782 (1993).
29. M. M. Howerton, G. K. Gopalakrishnan, R. P. Moeller, and W. K. Burns, "Low-biasing the cascaded downconverting fiber-optic link," in *Optical Fiber Communications, OFC.*, San Jose, CA, USA, (1996), pp. 211–213.
30. W. K. Burns, G. K. Gopalakrishnan, and R. P. Moeller, "Multi-octave operation of low-biased modulators by balanced detection," *IEEE Photonics Technol. Lett.* **8**(1), 130–132 (1996).
31. V. J. Urick, M. E. Godinez, P. S. Devgan, J. D. McKinney, and F. Bucholtz, "Analysis of an Analog Fiber-Optic Link Employing a Low-Biased Mach-Zehnder Modulator Followed by an Erbium-Doped Fiber Amplifier," *J. Lightwave Technol.* **27**(12), 2013–2019 (2009).
32. H. T. Friss, "Noise figures of radio receivers," *Proceeding of the IRE*, vol. **32**, no. 7, 1994.
33. W. Wei, L. Yi, Y. Jaouën, and W. Hu, "Software-defined microwave photonic filter with high reconfigurable resolution," *Sci. Rep.* **6**(1), 35621 (2016).
34. Keysight technologies selection guide, "Noise figure selection guide minimizing the uncertainties" (5989–8056EN. <http://literature.cdn.keysight.com/litweb/pdf/5989-8056EN.pdf>)

35. A. Choudhary, B. Morrison, I. Aryanfar, S. Shahnia, M. Pagani, Y. Liu, K. Vu, S. Madden, D. Marpaung, and B. J. Eggleton, "Advanced integrated microwave signal processing with giant on-chip Brillouin gain," *J. Lightwave Technol.* **35**(4), 846–854 (2017).